Functional, thermal and rheological properties of polymer-based magnetic composite filaments for additive manufacturing

Álvaro Díaz-García [a], Jia Yan Law [a], Manuel Felix [b], Antonio Guerrero [b], Victorino Franco [a,*]

[a] Departamento de Física de la Materia Condensada, ICMS-CSIC, Universidad de Sevilla, P.O. Box 1065, 41080 Sevilla, Spain
[b] Departamento de Ingeniería Química, Escuela Politécnica Superior, Universidad de Sevilla, 41011 Sevilla, Spain

HIGHLIGHTS

- Using polymer capsules filled with soft magnetic maraging steel particles as feedstock leads to the manufacturing of uniform magnetic filaments for 3D-printing.
- Magnetization of composite filament is proportional to the mass of magnetic fillers, where its demagnetizing factor remains independent of filler fraction.
- Metallic fillers act as nucleation centers favoring the formation of a disordered crystalline phase of polylactic acid polymer, and advances thermal degradation.
- The spherical fillers act as ball-bearings between polymer layers, reducing the melt viscosity of composites and leading to the lowering of printing temperature with respect to the pure polymer.

GRAPHICAL ABSTRACT
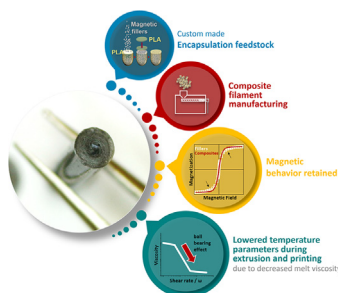
ARTICLE INFO

ABSTRACT

The design of functional composite filaments for fused filament fabrication requires a suitable polymer composition, functionality of particles, uniform distribution of fillers throughout the filament, and adequate printability. Uniform distribution at predictable concentrations is achieved by designing polymeric capsules containing the fillers and using them as feedstock for extrusion. Functionality can be inferred from that of the particles and target concentration. However, suitable conditions for printing strongly depend on polymer type and characteristics/concentration of fillers. Soft magnetic composite filaments were produced from polylactic acid (PLA) capsules filled with 30–52 wt. % maraging steel particles. Composite filaments preserve the soft magnetic character of the fillers. Fillers reduce the transition temperatures of the polymer by ~ 5 K and have a profound impact on printability. Rheological characterization shows that the "ball bearing effect" of gas-atomized particles reduces the viscosity of the composites by more than one order of magnitude, decreasing printing temperature from 215 °C to 170 °C, associated with the lack of agglomeration of particles achieved by the proposed production method. Rheological experiments allow to detect the required changes in printing conditions without requiring an extensive and costly trial and error process of printing with a large set of printing parameters.

* Corresponding author.
  E-mail address: vfranco@us.es (V. Franco).

1. Introduction

Additive manufacturing (AM) technologies are progressing rapidly and becoming a feasible alternative to traditional manufacturing processes due to various advantages (reduction of material waste, freedom of design, accessibility, etc.). However, important challenges remain, such as lower mechanical resistance of printed parts [1,2]. Among the different AM techniques, the most extended method is the fused deposition modeling (FDM), also known as fused filament fabrication (FFF). In this method, a filament (usually a thermoplastic) is fused and extruded for deposition in the form of thin layers, which builds a 3D object. Today, its ease of use has made it a popular choice, especially for printing parts made up of the typical polymers, such as PLA, ABS, PC, nylon, etc. However, parts are produced with relatively low mechanical strength and lack functional properties, being mainly used for developing structural models. A current line of interest in AM is the fabrication and use of composite functional filaments [3,4] as they can incorporate additional properties (e.g., magnetic [5–8], electrical [9–12], optical [13,14], etc.) to the FDM final printed parts suitable for 3D printing actuators, sensors, etc.

There are some commercial and tested composite filaments for functional applications. However, they are of limited varieties and compositions. Therefore, in many cases, custom-made composite filaments have to be manufactured to suit specific requirements. This implies the additional step of characterizing the prepared filaments as different additives can affect the properties of the polymer matrix in a very different way. On the one hand, mechanical properties and thermal behavior of composites can be improved with respect to the pure polymer with some types of reinforcement fillers, such as glass or carbon fibers [15–18], plasticizers [19], or polymer blends [20]. However, this is not the case with other types of additives in the composite filaments, where the filler fraction above a certain threshold will reduce the thermal stability and mechanical properties [21].

Regarding magnetic composite filaments, which could be used in numerous applications [22], the commercial stock is practically limited to polylactic acid (PLA) filled with $\sim$ 40 wt. % of iron particles (Proto-Pasta, produced by ProtoPlant, USA) or BASF Ultrafuse 17–4 PH, with a high load of 17–4 PH martensitic stainless steel (BASF, The Netherlands). Proto-pasta has been used in recent works due to its soft magnetic character [23–27] though the characteristics of the fillers are not ideal for functional applications as the iron particles are with inconsistent sizes and shapes [23,24] as well as easily rustable.

In a previous work, a procedure for obtaining homogeneous composite filaments at laboratory scale was presented [8], and its suitability for the purpose was demonstrated by fabricating filaments composed of PLA and soft magnetic maraging steel particles. PLA is a biodegradable polymer (under industrial composting conditions) [28], it is recyclable [29], and can be produced from starch sources such as potatoes, wheat, or corn. It is the most used thermoplastic in FDM due to its versatility and ease of processing. On the other hand, maraging steels are a class of low-carbon content steels known to exhibit good ductility and high strength from the precipitation of intermetallic phases. The alloying of Fe, Ni and Co as main constituents also provides a relevant ferromagnetic character to these steels. Therefore, maraging steels are widely used to build high performance components in applications that require the combination of high strength and magnetic properties, e.g., high-speed rotors, hysteresis motors, force-sensors, etc. [30–32].

In this work, a comprehensive characterization of PLA-based composite filaments with 30, 39 and 52 wt.% of gas-atomized magnetic maraging steel particles has been conducted by using

calorimetry, thermogravimetric analysis, dynamic mechanical analysis, shear rheology and magnetometry. The magnetic response of the composites is found to be proportional to the mass of fillers contained, having the same normalized performance in terms of a demagnetizing factor that is independent of the loading fraction. Regarding the processing characteristics of the composites, the thermal stability and mechanical properties of the PLA matrix are significantly affected by increasing the fraction of metallic fillers above 30%, altering the printing conditions of the filament. However, a good printability can be achieved even in the case of the highest loading fraction by conveniently modifying the printing parameters according to the results of the rheological characterization. Therefore, rheological characterization should be included in the design process of new printable materials to assess their printability in a more efficient way.

2. Experimental methods

The starting materials are standard grade PLA pellets (colorFabb B.V., The Netherlands) and maraging steel powder fabricated by gas atomization and sieved to 20 µm. X-ray tomography analysis reveals that the magnetic particle size distribution corresponds to a log-normal distribution with an average diameter of 6 µm and a variance of 4 µm, confirming that more than 99.5 % of particles exhibit diameters below the sieved size of 20 µm. This analysis also shows that particles have a high sphericity as 75 % of them exhibit sphericity values within the 0.9 – 1.0 range. More details about the morphology of the maraging steel particles that have been used as functional fillers for the composite filaments can be found in Ref. [8].

The manufacturing process of the composite filaments is summarized in Fig. 1 as follows: a PLA filament was manufactured using a single-screw desktop extruder NEXT 1.0 ADVANCED (3devo, The Netherlands) with the pre-installed settings for PLA standards. This filament was then subsequently used for 3D-printing PLA capsules and capsule lids (Fig. 1**a**)) with an Ultimaker S5 desktop printer (Ultimaker, The Netherlands). The printed PLA capsules were then filled with the magnetic particles, maraging steel powder, further sealed by the printed PLA lids for encapsulation (Fig. 1(**b**)). The sealed magnetic capsules act as the feedstock for extruding composite filaments with the abovementioned extruder (Fig. 1(**c**)). The described method allowed the development of homogeneous composite filaments (Fig. 1(**d**)) as the feedstock reached the melting and mixing areas of the extruder with constant concentration of the different components.

The functional magnetic properties have been investigated through magnetic field dependent magnetization measurements at room temperature using a Lake Shore Cryotronics 7407 vibrating sample magnetometer (VSM) (LakeShore, USA). Thermal characterization of samples from the different filaments was conducted by means of thermogravimetric analysis (TGA) using a Q600 (TA Instruments, USA) and by differential scanning calorimetry (DSC) using a DSC Q20 (TA Instruments, USA). TGA experiments were performed on samples of around 10 mg from room temperature up to 500 °C at a sweeping rate of 10 °C min^{-1} in N$_2$ atmosphere. DSC measurements were carried out upon heating from room temperature up to 200 °C at 10 °C min^{-1} in N$_2$ atmosphere with samples sealed in aluminum pans.

The evolution of the mechanical properties of the filament samples with temperature were analyzed by dynamic mechanical analysis (DMA) conducted using an RSA-III Solids Analyzer (TA Instruments, USA). 5 cm long sections of the filaments were prepared for these measurements, which were clamped in a cantilever tool in which the support and deformation points were fixed to the sample. The linear viscoelastic region (LVR) was determined by
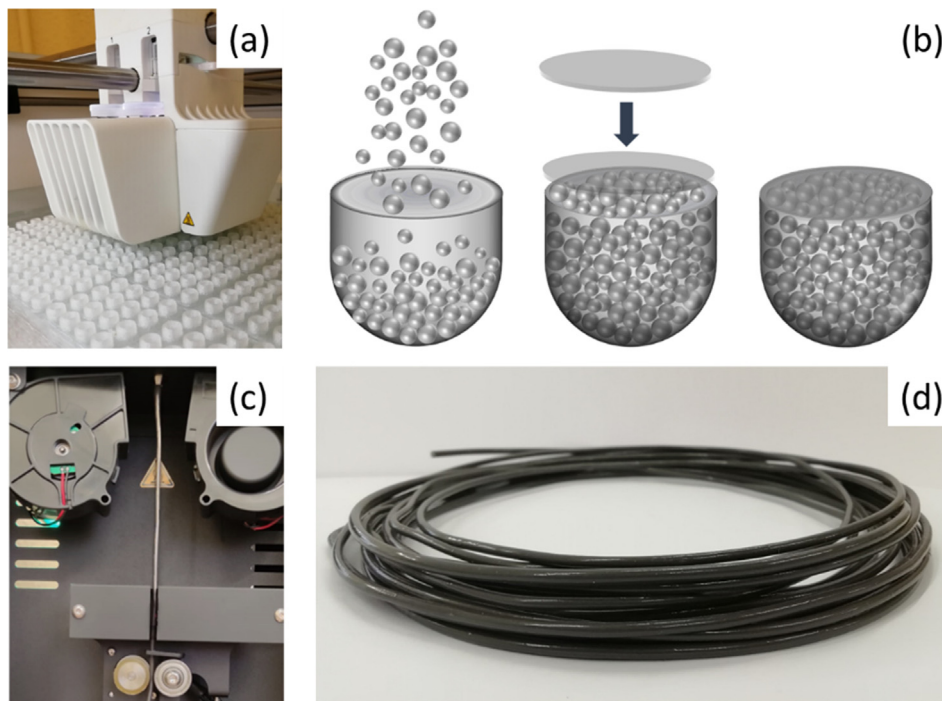
Fig. 1. Schematic representation of the fabrication of composite filaments: **(a)** 3D printing of PLA capsules, **(b)** filling up the polymeric capsules with functional fillers and sealing, **(c)** extrusion of the composite filament from the custom-made feedstock, and **(d)** an example of the final product that is an extrudable and spoolable composite filament of PLA and maraging steel particles.

strain sweep experiments at room temperature. Frequency tests at room temperature were also performed within the LVR by sweeping the frequency from 0.01 to 20 Hz. Temperature dependent DMA analyses were conducted in tension mode upon heating from room temperature at 5 °C min^{-1} for fixed strain within the LVR (0.02 %) and frequency (1 Hz).

Viscoelastic characterization of pure PLA and PLA-based composites were also assessed by small amplitude oscillatory shear (SAOS) measurements with a controlled stress rheometer DHR-3 (TA instruments, USA), using 40 mm parallel-plates configuration (1 mm gap). For SAOS experiments, pieces of PLA and composites were melted in a mold of ϕ 40 mm × 1 mm thickness to produce disc shapes to fit the dimensions of the parallel-plate configuration of the rheometer. The mechanical spectrum of the different specimens was obtained by sweeping the frequency from 0.05 to 10 rad s^{-1} at 70 °C (above the glass transition). For the measurements at 70 °C, samples were previously heated near the melting point to reach a highly rubbery state to adhere well to the sample holder plates at 70 °C without slipping. Frequency and flow tests were also conducted for melt samples at 160 °C. These frequency sweep tests were performed from 0.01 to 100 rad s^{-1}, while for the steady-state flow curves the rotation speed was swept from 0.01 to 30 rad s^{-1}.

3. Results and discussion

3.1. Functional magnetic properties

The magnetization (M) of the maraging steel powder (the functional filler for the composite filaments) and composite samples as a function of magnetic field (H) at room temperature are presented in Fig. 2**(a)**. The powder exhibits soft magnetic character with saturation magnetization at room temperature of 110.5 A m^2 kg^{-1} (for 1.5 T) and a negligible hysteresis of 2.81 mT.
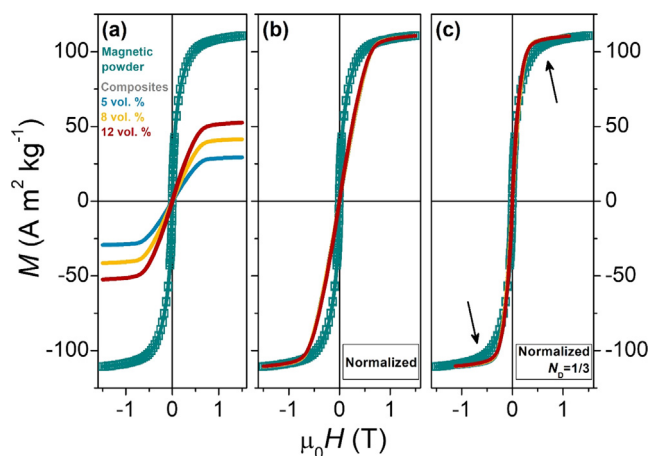

Fig. 2. (a) $M(H)$ loops of the raw magnetic steel powder (open square symbols) and samples from the three composite filaments (colored lines). **(b)** $M(H)$ curves normalized to the mass of magnetic particles. **(c)** Normalized $M(H)$ curves after correcting the demagnetizing factor of 1/3 for the samples of composite filaments. (For interpretation of the references to color in this figure legend, the reader is referred to the web version of this article).

Assuming that the measured magnetization of the composite filaments is exclusively due to the magnetic particles present within it, the mass fractions of fillers can be indirectly obtained from the comparison of the saturation magnetization per unit mass (for 1.5 T) with that of the starting powder. Nominal concentrations of fillers of 5, 8 and 12 vol. % correspond to 26.5, 37.5 and 47.5 wt. %, respectively. A further normalization of the magnetization curves of the composite filaments to the calculated filler mass shows a perfect correspondence among the curves as shown in Fig. 2**(b)**. When comparing the behavior of the normalized curves of the composites to that of the raw magnetic powder in Fig. 2 **(b)**, a good match is only observed in the saturation region above

0.75 T. Below that field, the magnetization curves of the composite samples differ from the steel powder, where those of composites show a more linear behavior with a significantly lower slope. The reason for this difference lies in the demagnetizing field. In the present case, all the samples correspond to magnetic particles with a high sphericity that are isotropically packed in a non-magnetic matrix. For these shapes of powdered magnetic samples, the effective demagnetizing factor can be approximated as [33]:

$$N \approx \frac{1}{3} + f \cdot \left(N_g - \frac{1}{3} \right), \tag{1}$$

where 1/3 corresponds to the demagnetizing factor of a sphere (in SI units), f is the packing fraction, and N_g is the demagnetizing factor of the geometry of the powder container.

In the case of the raw steel powder, ~ 4 mg was compacted in a silver capsule of 5 mm diameter at a maximum pressure of ~ 1 kbar. Its magnetization was measured with the field being applied parallel to the plane. Hence, this sample has an external shape that can be approximated without much error to that of a thin disc (i.e., a cylinder with a large diameter/length ratio, D/L) with highly packed particles. In the case of highly packed particles in which the sample container has a negligible demagnetizing factor, both terms $f \cdot N_g$ and $(1 - f)/3$ of **Eq. (1)** are expected to be irrelevant. A negligible demagnetizing factor for the compacted powder would agree to the experimental $M(H)$ loop as the large slope observed for low fields (i.e., a large susceptibility due to the applied field in the linear region) indicates that the demagnetizing field is not playing a relevant role.

On the other hand, samples of the composite filaments consist of cylindrical slices of ~ 3 mm diameter and a comparable length, in which particles are distributed with a relatively small packing fraction within the polymer matrix (f is as high as 0.12 for the filament with the largest filler content). The magnetic field in this case has also been applied perpendicular to the axis of the cylinder. Consequently, the use of a demagnetizing factor of 1/3 (spheres) is a good approximation because the second term $f \cdot (N_g - 1/3)$ in **Eq. (1)** is expected to be insignificant as f is relatively small. A common demagnetizing factor for the three different composites would agree with the normalized $M(H)$ curves in Fig. 2(**b**), which show the same slope regardless of the filler fractions. Fig. 2(**c**) shows the normalized curves after correcting the demagnetizing factor of the composite samples, together with the magnetization curve of the compacted powder. A better agreement with the response of the steel powder sample is now observed (comparing Fig. 2(**c**) and (**b**)), except for the curvature near saturation (marked with the arrows in Fig. 2(**c**)). This could be attributed to the different shape anisotropies of the compacted powder and filament samples as well as some minor changes in the magnetic anisotropy of the powder particles when subjected to the extrusion process. Temperatures of ~ 200 °C reached during the extrusion could also induce some stress relaxation of the maraging steel powder present in composite filaments.

The relatively uniform demagnetizing factor close to 1/3 for these filler concentrations makes that printed parts would also show an easily predictable $N = 1/3$ regardless of the final printed shape.

3.2. Thermal analysis

3.2.1. Thermogravimetric analysis (TGA)

The TGA results of the thermal degradation of the samples in the form of weight percent vs. temperature are shown in Fig. 3. As expected, the pure PLA sample completely degrades above 450 °C in a single step, having very minor remnant (lower than 0.5 wt. %) that can be due to minor fraction of ash. With respect
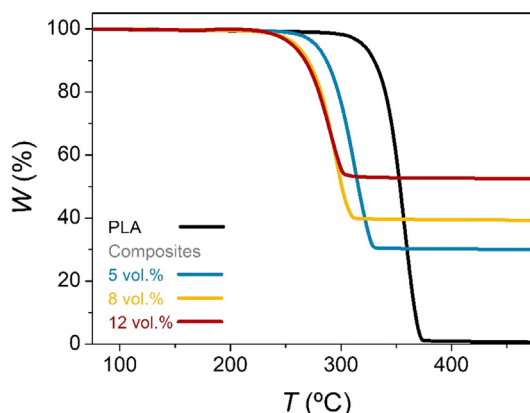

Fig. 3. TGA curves of PLA and of the different PLA/steel composites, indicating the weight percent of fillers. (For interpretation of the references to color in this figure legend, the reader is referred to the web version of this article).

to the samples of the composite filaments, the weight percent of fillers can be obtained as the remaining mass at the final temperature (fillers are nonvolatile in this temperature range), resulting in 30, 39 and 52 wt. % for the filaments with nominal 5, 8 and 12 vol. %, respectively. From this point, the composite filaments will be labeled by the wt. % of fillers obtained from the TGA measurements. The concentrations previously obtained from the magnetic measurements are in good agreement with the TGA results, noting that magnetic measurements underestimate the weight fraction of fillers by an average value of ~ 2 %. This can be due to the presence of oxides or small compositional variations in some particles, which can give lowered magnetic response. The results indicate that magnetization measurements can be useful for a quick investigation of the weight fraction of the magnetic filaments as this technique can give a good estimate, with the advantage that the measurements take lesser time and are non-destructive as compared to TGA investigations.

Apart from obtaining the filler fraction from the remaining mass upon the degradation of the polymer, TGA results can also reveal interesting features about the polymer degradation process associated to the presence of the fillers. It is evident from Fig. 3 that the onset of the mass loss is shifted to lower temperatures with increasing fraction of fillers. For a more detailed analysis, the temperature derivative of the weight percent is calculated and plotted in Fig. 4(**a**). The derivative curves confirm that the degradation of PLA occurs in a single step, with peak temperatures, T_{pk}, (i.e., the temperature at the maximum rate of mass change) shifting to lower values with increasing filler content. The shift of T_{pk} follows a nonlinear trend with filler content, being more than 40 °C below that of pure PLA compared to the 30 wt. % composite sample. However, for the composites with 39 and 52 wt. % of fillers, their T_{pk} values remain very close to each other. This indicates that the shift of T_{pk} slows down with the addition of fillers, becoming almost invariant above a certain filler fraction (the largest filler fraction in this study). Additionally, it can be noticed that the shapes of the different peaks in Fig. 4(**a**) are relatively similar for all cases, with the only evident differences detected for T_{pk} and peak values. A comparison of the kinetics of the degradation process for all the samples can be performed by normalizing the peaks using the derivative values at T_{pk} vs. a rescaled temperature axis ($T-T_{pk}$). The normalized curves are shown in Fig. 4(**b**), which verifies that all the peaks overlap. Therefore, this indicates that the steel particles just affect the temperatures at which the degradation of PLA takes place, with the kinetics of the process, once the degradation starts, being unaffected by the presence of these metallic fillers.
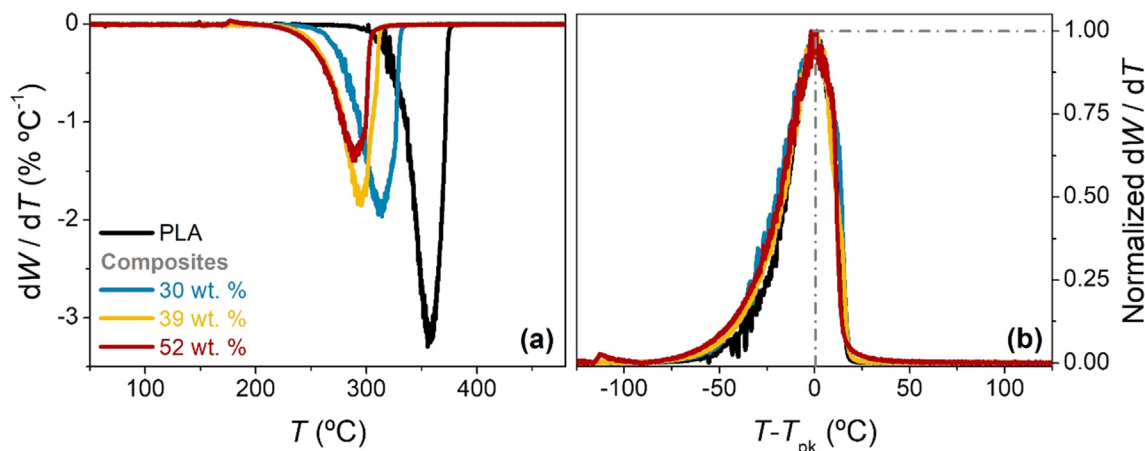
Fig. 4. (a) Derivative with respect to temperature of the TGA curves of PLA and the composites. **(b)** Normalized derivative curves vs. $T - T_{pk}$. (For interpretation of the references to color in this figure legend, the reader is referred to the web version of this article).

3.2.2. Differential scanning calorimetry (DSC)

DSC results of the first heating scan of pure PLA and composite filaments are shown in Fig. 5. To improve the visualization of the different features of the curves, they have been vertically shifted to prevent their overlap. For the pure PLA sample, the first observed features at ~ 60 °C arise due to the glass transition of the polymer. This indicates the transformation of the amorphous polymer from a rigid glassy state to a flexible and rubbery state due to the increasing molecular motion with temperature. The usual step in the heat flow baseline observed in a glass transition (due to a change of the heat capacity) is accompanied by an endothermic peak that indicates the presence of a relaxation process in which the amorphous polymer in a thermodynamically unstable state passes to a more stable state [34–36]. These observations at the glass transition temperature of PLA indicate that the polymer has been rapidly cooled below the glass transition temperature. The subsequent broad positive (exothermic) peak is attributed to the cold crystallization in which polymer crystals can be formed as the increased mobility of the molecules allows their rearrangement. The final endothermic peak is due to the melting of the polymer. The difference between the enthalpies related to melting and cold crystallization, ΔH_m and ΔH_{cc}, respectively (calculated through the integration of the corresponding heat flow peaks), can be used to estimate the percentage degree of crystallinity of the polymer, χ_c:

$$\chi_c = \frac{\Delta H_m - \Delta H_{cc}}{w_p \cdot \Delta H_m^0} \cdot 100, \tag{2}$$

where w_p is the weight fraction of polymer in the sample (ranging from 1 to 0.48 in this work), and ΔH_m^0 is the enthalpy of melting of the pure crystalline polymer [18,37,38]. In this case, the integration of the melting and cold crystallization peaks gives very similar values (within the error margin of the measurements) which implies a negligible χ_c and confirms that the polymer is mainly amorphous. This should be ascribed to the extrusion process, in which the fused filament is quickly cooled and solidified (i.e., quenched) after leaving the nozzle of the extruder, avoiding the formation of crystals.

The composite samples show the same qualitative characteristics, though quantitative differences are detected with respect to the curve of the pure PLA. The different transition temperatures (determined as the temperature at the corresponding peaks) are summarized in Table 1. The glass transition temperature (T_g) decreases with increasing filler fraction. A total decrease of more than 5 °C is observed between the T_g of the pure PLA and that of the composite filament with the highest filler fraction (52 wt. %).

The temperature of the peak corresponding to the cold crystallization (T_{cc}) of PLA is also affected by the addition of the metallic particles in a similar way as the T_g, decreasing as the filler concentration increases. In addition, the cold crystallization peak becomes sharper with increasing filler content. This indicates that the added metallic particles favor the crystallization of the polymer, acting as nucleation agents in agreement with literature [18,36,39,40]. Although these metallic fillers seem to promote crystallization of the polymer at those temperatures, the degree of crystallinity of PLA in the composite filaments using the fillers-encapsulation method proposed in [8] is still approximately zero.

Furthermore, the temperature of the peak associated to the melting of the polymer (T_m) shows the most obvious change with respect to the pure PLA as it splits into two overlapping but distin-
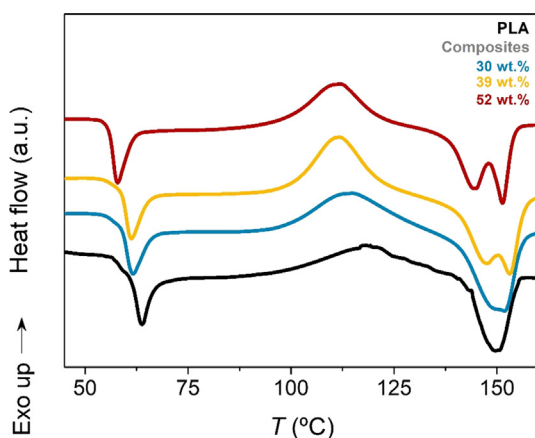

Fig. 5. Differential scanning calorimetry results upon heating of PLA and composite samples. (For interpretation of the references to color in this figure legend, the reader is referred to the web version of this article).

Table 1
Characteristics of the DSC peaks of the different transitions in samples labeled with the wt. % of maraging steel obtained from TGA measurements.

Sample	Glass transition T_g(°C)	Cold crystallization T_{cc}(°C)	Melting T_m(°C)
PLA	63.8	118.2	149.6
30 wt. %	61.8	115.0	149.3 – 151.5
39 wt. %	61.3	111.9	147.6 – 153.0
52 wt. %	57.8	111.9	144.4 – 151.4

guishable peaks with increasing filler fraction. This can be related to the formation of smaller and disordered crystalline lamellae during the crystallization of PLA, identified as disordered α′ phase, which has a lower melting point [36,39,40]. As the dispersed metallic particles act as nucleation centers, they could induce the formation of small and disordered crystallites around them, while larger and more ordered crystals can form in the bulk of polymeric matrix, giving rise to the observed split of the melting peak.

3.3. Rheological properties of PLA-based filaments

3.3.1. Influence of temperature on the dynamic mechanical properties

DMA tests are useful for characterizing the mechanical properties of polymeric materials, involving the measuring of the viscoelastic moduli at low constant frequency while varying the sample temperature. Interestingly, not only the mechanical response was obtained as a function of temperature, but also the values of glass transition temperature can be analyzed. Fig. 6 shows the response of the viscoelastic moduli (E' and E'') and tan (δ) (tan(δ) = E''/E') for the PLA and PLA-maraging steel filaments, where a remarkable effect of gas-atomized magnetic maraging steel particles (30, 39 and 52 wt. %) on the mechanical properties of the PLA-based filaments is observed. All the mechanical responses display a rigid glassy region at moderate temperature,
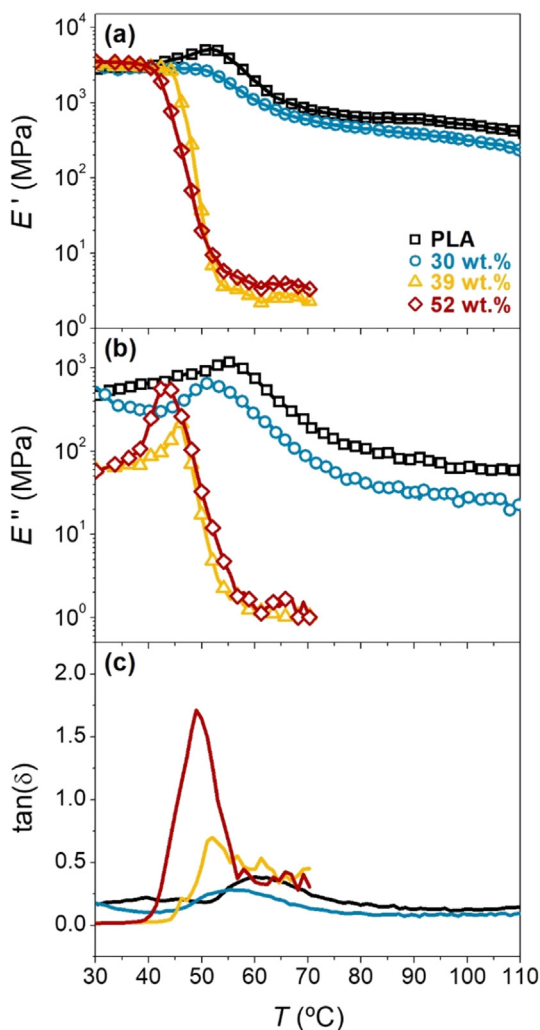

Fig. 6. Elastic (a), viscous (b) moduli, and tan(δ) (c) values as a function of temperature for PLA and composite samples. (For interpretation of the references to color in this figure legend, the reader is referred to the web version of this article).

where E' remains constant (up to ∼ 41 °C). While the pure PLA sample and the composite with the lowest fraction of particles (30 wt. %) show a quite similar behavior in this rigid glassy region, those with the higher particle fractions (i.e., 39 and 52 wt. %) show significant lower values of E'', indicating a lower capacity of energy dissipation. However, this effect became weaker with increasing temperature, showing a maximum value in E''.

The glassy region was followed by a transition region, reflected by a decrease in the viscoelastic moduli as temperature increased (Fig. 6(**a**) and **6(b)**). A characteristic inflection point attributed to a T_g can be identified in this region. This glass transition temperature can also be determined by the maximum peak observed in tan (δ) (Fig. 6(**c**)). Although all the systems exhibited an overall similar response, the intensity of the response significantly varied with the addition of metallic particles. Thus, two different thermal profiles can be observed. On the one hand, systems without particles or low particle concentration (up to 30 wt. %) exhibited a quite similar moderate decrease in E' and E'' values after the glass transition temperature. In contrast, higher particle concentrations (i.e., 39 and 52 wt. %) led to a dramatic drop in the viscoelastic moduli (particularly in E'). The transition region, which was narrower for the latter case, gave rise to a broad rubbery plateau region at high temperatures. The viscoelastic properties at the plateau region also depended on the particle concentration (e.g., E' was reduced from 708 ± 25 MPa s for PLA to 3.50 ± 0.32 MPa s for PLA filament containing 52 wt. % particles). Jain et al [41] also found a decrease in the viscoelastic moduli for polypropylene samples filled with silica nanoparticles. This effect can be ascribed to a distortion of the polymer network caused by increasing particle content.

Regarding the tan(δ) curves, an evident peak appeared at the glass transition temperature of the different studied systems. In accordance with results from DSC, the addition of particles shifted the glass transition to lower temperatures (from 60 to 49 °C for the PLA and PLA-52 wt. % particles, respectively). It can be noticed that the T_g values obtained from tan(δ) are lower than those obtained from DSC profiles, however it should be borne in mind that the heating rate for DMA tests was half the value of the heating rate for DSC measurements.

3.3.2. Viscoelastic characterization by shear rheology

The dependence of viscoelastic moduli on angular frequency at 70 °C for PLA and composites samples is shown in Fig. 7 (**a**), which helps to analyze the mechanical behavior of the polymer and composite samples much below the melting point. The viscoelastic response observed for PLA is typical of high molecular weight polymers, covering the shift from the plateau to the rubbery region, which is related to the crossover point between elastic (G') and viscous (G'') moduli. The plateau region, where the elastic modulus dominates, can be observed at low frequencies, whereas the viscous modulus dominates at short relaxation time (high frequencies) in the rubbery zone [42]. This behavior changes depending on the filler content. The composite with the lowest concentration (30 wt. %) shows a similar behavior to PLA, where the crossover point is displaced towards higher frequencies, even though the plateau region seems to undergo a slight shrinkage. Further increase in particle content leads to progressive changes. Thus, the shrinkage of the plateau region becomes evident for the composite containing 39 wt. % particles and disappears for the highest content. As a result, G' does not become dominant over the whole frequency window for the composite containing 52 wt. %, which agrees with the low values previously observed for the temperature ramp tests. The viscoelastic functions have been previously used for analyzing the compatibility of polymer blends [43,44]. In this case, the number of particles in the filled polymers seems to reduce the polymer–polymer interactions, leading to a predominant fluid behavior (for the sample containing 52 wt. % maraging particles) [45].
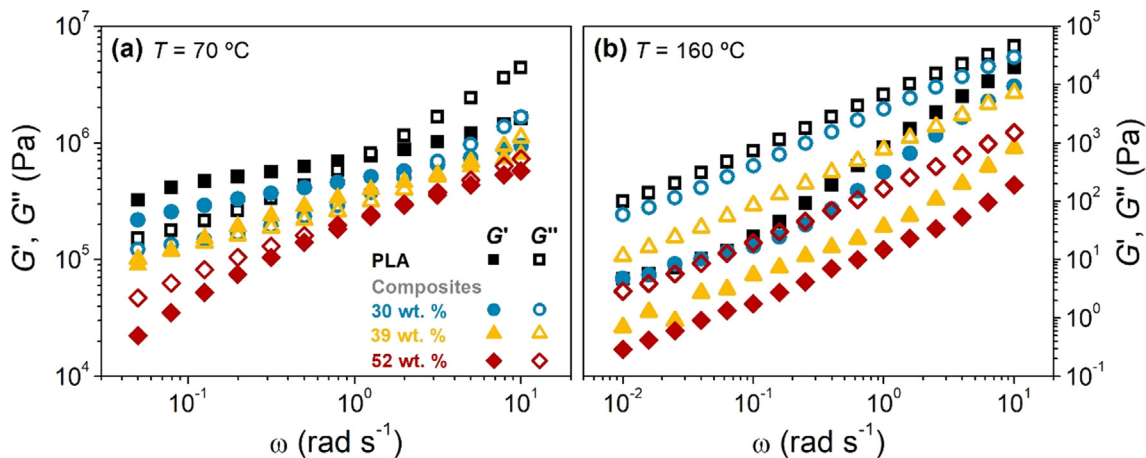
Fig. 7. **(a)** Viscoelastic moduli as a function of the angular frequency (ω) at 70 °C for PLA and composite samples. **(b)** Viscoelastic moduli as a function of angular frequency at 160 °C for PLA and composite samples. (For interpretation of the references to color in this figure legend, the reader is referred to the web version of this article).

The dependence of viscoelastic moduli on frequency at 160 °C for PLA and composites samples is shown in Fig. 7 **(b)**, helping to analyze the microstructures of the melted polymer and composite samples, where the interactions between particles and polymer–polymer chains influenced the obtained response. The analysis by small amplitude oscillatory shear (SAOS) rheology indicates that both viscoelastic functions exhibit a strong frequency dependence. The viscous component predominates over the elastic component for all the samples. This result reflects a typical behavior of the terminal zone of the linear relaxation spectrum and is in agreement with other results obtained for thermoplastic polymer melts, where the viscous component is also predominant [46]. It is worth pointing out the remarkable decrease in the viscoelastic moduli at the fused state as the particle content increases. These results suggest that the filler addition increases the fluid character of the melted polymer. Thus, the addition of maraging particles not only affects the rheological properties of the polymer in the glassy and rubbery states, but it also affects the flow region above the melting point, changing the conditions for a proper processability of the fused composite filaments compared to pure PLA. Therefore, the polymer molecular microstructure and the flow properties of the polymer and composite melts were subsequently analyzed by steady-state flow tests.

A comparison between the complex viscosity (η*) from SAOS tests and the apparent viscosity (η) from steady-state flow measurements reveals that neither the PLA nor the PLA-based composites analyzed in this work follow the Cox-Merz rule:

$$\eta^*(\omega) = \eta(\dot{\gamma} = \omega), \tag{3}$$

where $\dot{\gamma}$ is the shear rate in the steady-state flow measurements. This is in contrast with the good fitting reported by some authors for melted PLA [47,48]. However, a modified Cox-Merz rule can be used for the samples in this study [49]:

$$\eta^*(\omega) \cdot A = \eta(\dot{\gamma} = \omega), \tag{4}$$

where A is a dimensionless parameter that accounts for the effect of shear forces on the unperturbed microstructure of the system.

Fig. 8 shows the complex viscosity and the multiplication of the complex viscosity and parameter A as a function of frequency and shear rate, respectively. As observed, all the systems follow the modified Cox-Merz rule (**Eq. (4)**), using the same value of A = 0.59 regardless of particle concentration and the type of shear deformation applied (steady or oscillatory). This figure confirms the reduction of the rheological properties (also for the apparent
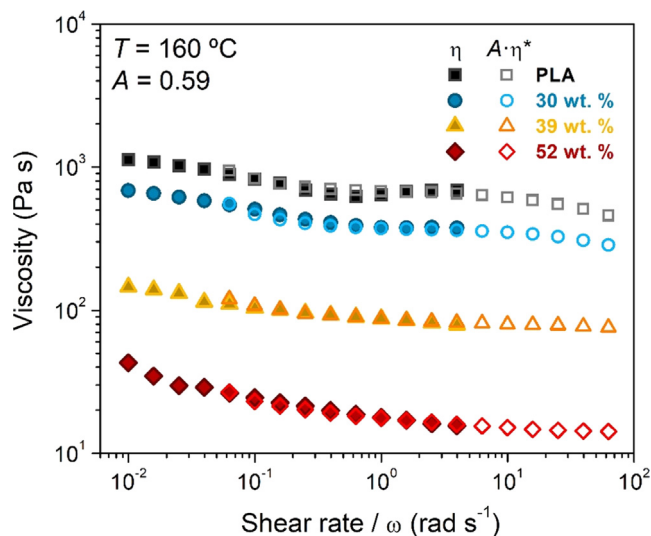

Fig. 8. Apparent (η) and complex (A·η*) viscosities obtained for PLA and composite samples at 160 °C. (For interpretation of the references to color in this figure legend, the reader is referred to the web version of this article).

viscosity) with increasing particle content. Typically, the flow viscosity of filler-containing polymers increases with filler concentration [50–52]. However, a reduction in viscosity with the addition of fillers has also been reported for calcium carbonate in PVC [53] and glass beads in polycarbonate [54], agreeing with the results obtained for PLA containing maraging steel particles in this work. These authors attributed the viscosity decrease to the reduction of the interlayer interactions of the melt polymer with the spherical particles, corresponding to the so-called "ball-bearing" effect, which is more pronounced with increasing filler content. This effect was observed not only for high shear capillary viscosity but also for shear rheology at lower shear rates. Shenoy [55] also reported this effect in carbon-black polymer textures, being interpreted as an internal reduction in friction between the polymer chains by the spherical particles, which act as ball-bearings for the adjacent polymeric matrix.

Moreover, these results agree with those obtained from SAOS measurements. Chang et al. [54] employed the comparison of SAOS and flow viscosity results to analyze the possible arrangement of particles through the polymer network. They found a reduction in the zero-shear viscosity at a volume particle content in the order

of those used in this study (~10 vol. %). In that case, only weak particle aggregates were formed and the ball-bearing effect dominates, leading to a reduction in viscosity. An increase in viscosity driven by particle aggregation was only found to be dominant at higher particle concentrations (greater than 20 vol. %), which are far from those studied in this work.

According to these results, it is clear that the particle content is a factor that notably affects the printability of the composite filaments. In this case, the decrease in viscosity with the addition of fillers agrees with previous work where it was necessary to lower both the temperature for the manufacturing of the filaments and the printing temperature with respect to those of pure PLA. For the manufacturing of the filaments, a drastic reduction of the temperature of the different heating stages along the extrusion path was necessary so that the composite filaments do not exit the nozzle in such a fluid state that prevented them to be spooled. The same applies for their printing, as the temperature had to be lowered from 215 °C (default for PLA) to 170 °C to be able to print with the composites. Just by lowering the extrusion temperature, the composite filaments could be spooled and used for 3D-printing. The high flowability of melted composite filaments and the low rate of particle agglomeration achieved by the adopted filament manufacturing process [8] prevented the usual nozzle clogging. The results from the viscoelastic experiments suggest that further increase of the particle content could lead to an increase of the viscosity if the particle agglomeration becomes predominant over the "ball-bearing" effect, making the composite approach again to the viscosity of pure PLA. However, the used particle fractions together with the manufacturing method seem to be a good combination for the fabrication of composite filaments with uniform functional properties as the particle agglomeration is negligible as well as the rheological properties do not excessively hinder their printability.

4. Conclusions

Through a novel procedure based on the use of filled polymer capsules as the feedstock for extrusion, composite filaments combining PLA and soft magnetic maraging steel particles (30, 39 and 52 wt. %) were manufactured for the 3D-printing of magnetic functional parts. In this work, the different properties of the filaments have been systematically studied. Magnetic hysteresis loops confirm that the composites preserve the soft magnetic character of the magnetic powder, with the only difference being the demagnetizing factor, which remains constant (~1/3) for the different filler fractions. Special attention is paid to the factors that might affect the printability of the filaments and the suitable printing conditions. The metallic fillers significantly affect and shift the different thermal processes that the polymer undergoes until its final degradation at high temperatures. The results of rheological characterization of PLA and PLA-based composites directly explain the reasons for the change in the extrudability and printability of the composites filaments with respect to pure PLA. The "ball-bearing effect" caused by the almost spherical gas atomized particles produces an abrupt drop of the viscosity of the composite with respect to that of pure PLA for the same temperature, which requires the lowering of the extrusion and printing temperatures to achieve an appropriate viscosity for the processing of the fused filaments. It is also worth mentioning that the lowered temperature required for fabrication and printing entails a reduction of the energy costs associated with the additive manufacturing process.

CRediT authorship contribution statement

Álvaro Díaz-García: Conceptualization, Methodology, Formal analysis, Investigation, Writing – original draft, Writing – review & editing. **Jia Yan Law:** Conceptualization, Methodology, Investigation, Writing – review & editing, Supervision. **Manuel Felix:** Formal analysis, Investigation, Writing – review & editing. **Antonio Guerrero:** Formal analysis, Investigation, Writing – review & editing. **Victorino Franco:** Conceptualization, Methodology, Investigation, Writing – review & editing, Supervision, Funding acquisition.

Data Availability.

The data that support the findings of this study are available upon reasonable request.

Declaration of Competing Interest

The authors declare that they have no known competing financial interests or personal relationships that could have appeared to influence the work reported in this paper.

Acknowledgements

References

[1] T.D. Ngo, A. Kashani, G. Imbalzano, K.T.Q. Nguyen, D. Hui, Additive manufacturing (3D printing): A review of materials, methods, applications and challenges, Compos Part B Eng 143 (2018) 172–196, https://doi.org/10.1016/j.compositesb.2018.02.012.

[2] S.A.M. Tofail, E.P. Koumoulos, A. Bandyopadhyay, S. Bose, L. O'Donoghue, C. Charitidis, Additive manufacturing: scientific and technological challenges, market uptake and opportunities, Mater. Today 21 (2018) 22–37, https://doi.org/10.1016/j.mattod.2017.07.001.

[3] X. Wang, M. Jiang, Z. Zhou, J. Gou, D. Hui, 3D printing of polymer matrix composites: A review and prospective, Compos Part B Eng 110 (2017) 442–458, https://doi.org/10.1016/j.compositesb.2016.11.034.

[4] P.M. Angelopoulos, M. Samouhos, M. Taxiarchou, Functional fillers in composite filaments for fused filament fabrication: A review, Mater. Today:. Proc. 37 (2019) 4031–4043, https://doi.org/10.1016/j.matpr.2020.07.069.

[5] C. Huber, C. Abert, F. Bruckner, M. Groenefeld, S. Schuschnigg, I. Teliban, C. Vogler, G. Wautischer, R. Windl, D. Suess, 3D Printing of Polymer-Bonded Rare-Earth Magnets with a Variable Magnetic Compound Fraction for a Predefined Stray Field, Sci. Rep. 7 (1) (2017), https://doi.org/10.1038/s41598-017-09864-0.

[6] A.P. Taylor, C. Velez Cuervo, D.P. Arnold, L.F. Velasquez-Garcia, Fully 3D-printed, monolithic, mini magnetic actuators for low-cost, compact systems, J Microelectromechanical Syst 28 (2019) 481–493, https://doi.org/10.1109/JMEMS.2019.2910215.

[7] R.P. Magisetty, N.S. Cheekuramelli, Additive manufacturing technology empowered complex electromechanical energy conversion devices and transformers, Appl. Mater. Today 14 (2019) 35–50, https://doi.org/10.1016/j.apmt.2018.11.004.

[8] Á. Díaz-García, J.Y. Law, A. Cota, A. Bellido-Correa, J. Ramírez-Rico, R. Schäfer, V. Franco, Novel procedure for laboratory scale production of composite functional filaments for additive manufacturing, Mater. Today Commun. 24 (2020) 101049.

[9] S.W. Kwok, K.H.H. Goh, Z.D. Tan, S.T.M. Tan, W.W. Tjiu, J.Y. Soh, Z.J.G. Ng, Y.Z. Chan, H.K. Hui, K.E.J. Goh, Electrically conductive filament for 3D-printed circuits and sensors, Appl. Mater. Today 9 (2017) 167–175.

[10] A. Dorigato, V. Moretti, S. Dul, S.H. Unterberger, A. Pegoretti, Electrically conductive nanocomposites for fused deposition modelling, Synth. Met. 226 (2017) 7–14, https://doi.org/10.1016/j.synthmet.2017.01.009.

[11] K. Gnanasekaran, T. Heijmans, S. van Bennekom, H. Woldhuis, S. Wijnia, G. de With, H. Friedrich, 3D printing of CNT- and graphene-based conductive polymer nanocomposites by fused deposition modeling, Appl. Mater. Today 9 (2017) 21–28.

[12] T.M. Calascione, N.A. Fischer, T.J. Lee, H.G. Thatcher, B.B. Nelson-Cheeseman, Controlling magnetic properties of 3D-printed magnetic elastomer structures via fused deposition modeling, AIP Adv. 11 (2) (2021) 025223.

[13] T. Rimpongpisarn, W. Wattanathana, K. Sukthavorn, N. Nootsuwan, Y. Hanlumyuang, C. Veranitisagul, A. Laobuthee, Novel luminescent PLA/MgAl2O4:Sm3+ composite filaments for 3D printing application, Mater. Lett. 237 (2019) 270–273.

[14] M. Wan, X. Jiang, J. Nie, Q. Cao, W. Zheng, X. Dong, Z.H. Fan, W. Zhou, Phosphor powders-incorporated polylactic acid polymeric composite used as 3D printing filaments with green luminescence properties, J. Appl. Polym. Sci. 137 (18) (2020) 48644.

[15] F. Ning, W. Cong, J. Qiu, J. Wei, S. Wang, Additive manufacturing of carbon fiber reinforced thermoplastic composites using fused deposition modeling, Compos Part B Eng 80 (2015) 369–378, https://doi.org/10.1016/j.compositesb.2015.06.013.

[16] P. Parandoush, D. Lin, A review on additive manufacturing of polymer-fiber composites, Compos. Struct. 182 (2017) 36–53, https://doi.org/10.1016/j.compstruct.2017.08.088.

[17] J.M. Chacón, M.A. Caminero, P.J. Núñez, E. García-Plaza, I. García-Moreno, J.M. Reverte, Additive manufacturing of continuous fibre reinforced thermoplastic composites using fused deposition modelling: Effect of process parameters on mechanical properties, Compos. Sci. Technol. 181 (2019), https://doi.org/10.1016/j.compscitech.2019.107688 107688.

[18] L. Sang, S. Han, X. Peng, X. Jian, J. Wang, Development of 3D-printed basalt fiber reinforced thermoplastic honeycombs with enhanced compressive mechanical properties, Compos Part A Appl Sci Manuf 125 (2019), https://doi.org/10.1016/j.compositesa.2019.105518 105518.

[19] Y.S. Ko, D. Herrmann, O. Tolar, W.J. Elspass, C. Brändli, Improving the filament weld-strength of fused filament fabrication products through improved interdiffusion, Addit. Manuf. 29 (2019), https://doi.org/10.1016/j.addma.2019.100815 100815.

[20] A.S. de León, A. Domínguez-Calvo, S.I. Molina, Materials with enhanced adhesive properties based on acrylonitrile-butadiene-styrene (ABS)/thermoplastic polyurethane (TPU) blends for fused filament fabrication (FFF), Mater. Des. 182 (2019), https://doi.org/10.1016/j.matdes.2019.108044 108044.

[21] S. Hwang, E.I. Reyes, K.-S. Moon, R.C. Rumpf, N.S. Kim, Thermo-mechanical Characterization of Metal/Polymer Composite Filaments and Printing Parameter Study for Fused Deposition Modeling in the 3D Printing Process, J. Electron. Mater. 44 (3) (2015) 771–777.

[22] S. Banerjee, A.K. Tyagi, Functional Materials, Elsevier (2012), https://doi.org/10.1016/C2010-0-65659-8.

[23] L.M. Bollig, P.J. Hilpisch, G.S. Mowry, B.B. Nelson-Cheeseman, 3D printed magnetic polymer composite transformers, J. Magn. Magn. Mater. 442 (2017) 97–101, https://doi.org/10.1016/j.jmmm.2017.06.070.

[24] L.M. Bollig, M.V. Patton, G.S. Mowry, B.B. Nelson-Cheeseman, Effects of 3-D Printed Structural Characteristics on Magnetic Properties, IEEE Trans. Magn. 53 (11) (2017) 1–6.

[25] S. Fafenrot, N. Grimmelsmann, M. Wortmann, A. Ehrmann, Three-dimensional (3D) printing of polymer-metal hybrid materials by fused deposition modeling, Materials (Basel) 10 (2017) 1199, https://doi.org/10.3390/ma10101199.

[26] M.V. Patton, P. Ryan, T. Calascione, N. Fischer, A. Morgenstern, N. Stenger, et al., 3D printed magnetic polymer composite transformers, Addit. Manuf. 27 (2018) 97–101, https://doi.org/10.1016/j.addma.2018.06.009.

[27] M.V. Patton, P. Ryan, T. Calascione, N. Fischer, A. Morgenstern, N. Stenger, B.B. Nelson-Cheeseman, Manipulating magnetic anisotropy in fused filament fabricated parts via macroscopic shape, mesoscopic infill orientation, and infill percentage, Addit. Manuf. 27 (2019) 482–488.

[28] E. Castro-Aguirre, R. Auras, S. Selke, M. Rubino, T. Marsh, Enhancing the biodegradation rate of poly(lactic acid) films and PLA bio-nanocomposites in simulated composting through bioaugmentation, Polym. Degrad. Stab. 154 (2018) 46–54, https://doi.org/10.1016/j.polymdegradstab.2018.05.017.

[29] P. Zhao, C. Rao, F. Gu, N. Sharmin, J. Fu, Close-looped recycling of polylactic acid used in 3D printing: An experimental investigation and life cycle assessment, J Clean Prod 197 (2018) 1046–1055, https://doi.org/10.1016/j.jclepro.2018.06.275.

[30] J.M. Pardal, S.S.M. Tavares, M.P. Cindra Fonseca, M.R. Da Silva, J.M. Neto, H.F.G. Abreu, Influence of temperature and aging time on hardness and magnetic properties of the maraging steel grade 300, J. Mater. Sci. 42 (2007) 2276–2281, https://doi.org/10.1007/s10853-006-1317-8.

[31] G.C.S. Nunes, P.W.C. Sarvezuk, T.J.B. Alves, V. Biondo, F.F. Ivashita, A. Paesano, Maraging-350 steel: Following the aging through diffractometric, magnetic and hyperfine analysis, J. Magn. Magn. Mater. 421 (2017) 457–461, https://doi.org/10.1016/j.jmmm.2016.08.052.

[32] G.V. Thotakura, R. Goswami, T.V. Jayaraman, Structure and magnetic properties of milled maraging steel powders, Powder Technol. 360 (2020) 80–95, https://doi.org/10.1016/j.powtec.2019.09.054.

[33] Coey JMD. Magnetism and Magnetic Materials. Cambridge University Press; 2001. 10.1017/CBO9780511845000.

[34] P. Pan, B. Zhu, Y. Inoue, Enthalpy relaxation and embrittlement of poly(L-lactide) during physical aging, Macromolecules 40 (2007) 9664–9671, https://doi.org/10.1021/ma071777c.

[35] M. Kwon, S.C. Lee, Y.G. Jeong, Influences of physical aging on enthalpy relaxation behavior, gas permeability, and dynamic mechanical property of polylactide films with various D-isomer contents, Macromol. Res. 18 (2010) 346–351, https://doi.org/10.1007/s13233-010-0410-7.

[36] B. Coppola, N. Cappetti, M.L. Di, P. Scarfato, L. Incarnato, 3D printing of PLA/clay nanocomposites: Influence of printing temperature on printed samples properties, Materials (Basel) 11 (2018) 1–17, https://doi.org/10.3390/ma11101947.

[37] Y. Kong, J.N. Hay, The measurement of the crystallinity of polymers by DSC, Polymer (Guildf) 43 (2002) 3873–3878, https://doi.org/10.1016/S0032-3861(02)00235-5.

[38] Y. Song, Y. Li, W. Song, K. Yee, K.-Y. Lee, V.L. Tagarielli, Measurements of the mechanical response of unidirectional 3D-printed PLA, Mater. Des. 123 (2017) 154–164, https://doi.org/10.1016/j.matdes.2017.03.051.

[39] F.S. Senatov, K.V. Niaza, M.Y. Zadorozhnyy, A.V. Maksimkin, S.D. Kaloshkin, Y.Z. Estrin, Mechanical properties and shape memory effect of 3D-printed PLA-based porous scaffolds, J. Mech. Behav. Biomed. Mater. 57 (2016) 139–148, https://doi.org/10.1016/j.jmbbm.2015.11.036.

[40] A. Karakoç, V.K. Rastogi, T. Isoaho, B. Tardy, J. Paltakari, O.J. Rojas, Comparative Screening of the Structural and Thermomechanical Properties of FDM Filaments Comprising Thermoplastics Loaded with Cellulose, Carbon and Glass Fibers. Materials (Basel) 13 (2020) 422, https://doi.org/10.3390/ma13020422.

[41] S. Jain, J.G.P. Goossens, G.W.M. Peters, M. van Duin, P.J. Lemstra, Strong decrease in viscosity of nanoparticle-filled polymer melts through selective adsorption, Soft Matter 4 (2008) 1848–1854, https://doi.org/10.1039/B802905A.

[42] W.D. Cook, T.F. Scott, S. Quay-Thevenon, J.S. Forsythe, Dynamic mechanical thermal analysis of thermally stable and thermally reactive network polymers, J. Appl. Polym. Sci. 93 (2004) 1348–1359, https://doi.org/10.1002/app.20569.

[43] B. Nandan, L.D. Kandpal, G.N. Mathur, Poly(ether ether ketone)/poly(aryl ether sulfone) blends: Melt rheological behavior, J Polym Sci Part B-Polymer Phys 42 (2004) 1548–1563, https://doi.org/10.1002/polb.20039.

[44] K. Urman, J.U. Otaigbe, New phosphate glass/polymer hybrids—Current status and future prospects, Prog. Polym. Sci. 32 (2007) 1462–1498, https://doi.org/10.1016/j.progpolymsci.2007.07.006.

[45] Y. Song, L. Zeng, Q. Zheng, Reconsideration of the Rheology of Silica Filled Natural Rubber Compounds, J. Phys. Chem. B 121 (2017) 5867–5875, https://doi.org/10.1021/acs.jpcb.7b02760.

[46] A. Santamaria, M.E. Muñoz, M. Fernández, M. Landa, Electrically conductive adhesives with a focus on adhesives that contain carbon nanotubes, J. Appl. Polym. Sci. 129 (2013) 1643–1652, https://doi.org/10.1002/app.39137.

[47] H.J. Lehermeier, J.R. Dorgan, Melt rheology of poly(lactic acid): Consequences of blending chain architectures, Polym. Eng. Sci. 41 (2001) 2172–2184, https://doi.org/10.1002/pen.10912.

[48] I.H. Park, J.Y. Lee, S.J. Ahn, H.J. Choi, Melt Rheology and Mechanical Characteristics of Poly(Lactic Acid)/Alkylated Graphene Oxide Nanocomposites, Polymers (Basel) 12 (10) (2020) 2402.

[49] K.C. Tam, C. Tiu, Modified cox-merz rule for charged polymer systems in solution, J Macromol Sci Part B 33 (1994) 173–184, https://doi.org/10.1080/00222349408248086.

[50] L.A. Faitel'son, A.I. Alekseenko, Effect of fillers on the viscosity and viscoelasticity of low-density polyethylene melts, Communication 1. Polym Mech 12 (3) (1977) 430–438.

[51] L.A. Utracki, The Shear and Elongational Flow of Polymer Melts Containing Anisometric Filler Particles, Part I. Rubber Chem Technol 57 (1984) 507–522, https://doi.org/10.5254/1.3536018.

[52] G. Akay, Flow induced polymer-filler interactions: Bound polymer properties and bound polymer-free polymer phase separation and subsequent phase inversion during mixing, Polym. Eng. Sci. 30 (1990) 1361–1372, https://doi.org/10.1002/pen.760302106.

[53] X.-L. Xie, Q.-X. Liu, R.-Y. Li, X.-P. Zhou, Q.-X. Zhang, Z.-Z. Yu, Y.-W. Mai, Rheological and mechanical properties of PVC/CaCO3 nanocomposites prepared by in situ polymerization, Polymer (Guildf) 45 (19) (2004) 6665–6673.

[54] P. Chen, J. Zhang, J. He, Increased flow property of polycarbonate by adding hollow glass beads, Polym. Eng. Sci. 45 (2005) 1119–1131, https://doi.org/10.1002/pen.20382.

[55] Shenoy A V. Rheology of Filled Polymer Systems. 1st ed. Dordrecht: Springer Netherlands; 1999. 10.1007/978-94-015-9213-0.